



OPEN

Matrix metalloproteinase-2 as a novel regulator of glucose utilization by adipocytes

Melissa D. Lempicki¹, Ryan J. Garrigues², Alexander D. Hondros², Tonya N. Zeczycki², Brandon L. Garcia³, John Cavanagh², Thurl E. Harris⁴ & Akshaya K. Meher¹✉

Glucose transporter 4 (GLUT4) expression on white adipocytes is critical for facilitating cellular uptake of blood glucose, failure of which promotes hyperglycemia. Matrix metalloproteinases (MMPs) play a crucial role in remodeling the white adipose tissue (WAT) during obesity. MMPs have multiple protein substrates, and surprisingly, it is unknown if they can directly target GLUT4 on the adipocyte surface and impair glucose uptake. We identified MMP2 as the highly active gelatinase, a class of MMP, in the gonadal WAT of high-fat diet-induced obese mice. *In vitro*, metabolic studies in 3T3-L1 adipocytes revealed MMP2 attenuated glucose uptake and glycolysis, which were recovered by an MMP2 inhibitor. *In silico* structural analysis using AlphaFold identified a putative MMP2 cleavage site on the extracellular domain of GLUT4. Further, in a substrate competition assay, a peptide mimicking the MMP2 cleavage site on GLUT4 attenuated the cleavage of an MMP substrate by MMP2. Altogether, our results suggest a novel mechanism of impaired glucose utilization by adipocytes, which may contribute to hyperglycemia during obesity.

Obesity and its related comorbidity insulin resistance (IR), pose a significant health risk in developed countries. While many factors contribute to the development of IR, murine models of high-fat diet (HFD)-induced obesity revealed that glucose transporter 4 (GLUT4) expression on white adipocytes promotes insulin-stimulated glucose uptake and maintenance of whole-body glucose homeostasis¹. During obesity, GLUT4 expression on the surface of adipocytes decreases, leading to hyperglycemia and eventually IR². Matrix metalloproteinases (MMPs), a family of over 23 zinc-dependent endoproteinases, play a crucial role in remodeling the extracellular matrix of the white adipose tissue (WAT) during obesity³. While MMPs are crucial for matrix remodeling, it is unknown whether MMPs directly affect adipocyte function and metabolism by degrading GLUT4 on the adipocyte surface.

Here, we identified MMP2 as the highly active gelatinase, a class of MMP, in the gonadal WAT of obese mice and determined if MMP2 directly affects adipocyte glucose utilization using 3T3-L1 adipocytes.

Results

MMP2 is the highly active gelatinase in white adipose tissue during obesity

In obese and IR humans and mice, macrophages infiltrate the adipose tissue and produce pro-inflammatory cytokines that can exacerbate IR development⁴. Furthermore, plasma MMP levels, ranging from 100 to 400 ng/mL in non-obese patients and over 1 µg/mL in obese patients, correlate with several obesity-related parameters^{5,6}. To determine the highly active gelatinase in the WAT during HFD-induced obesity, we placed male C57BL/6J mice on an HFD for 5, 9, or 11 weeks or NCD for 11 weeks. As expected, the mice on HFD had increased body weight, increased fasting insulin levels, and reduced AKT phosphorylation in the gonadal WAT (Sup. Figure 1A–C). Apart from this, mice 11 weeks on HFD had an increase in the percent of total macrophages and an increase in expression of CD86, a marker for pro-inflammatory M1 macrophages, and an increase in the *Tnfα* gene expression in the stromal vascular fraction of the gonadal WAT (Sup. Figure 1D–F). Furthermore, the number of crown-like structures (CLSs) was increased in the gonadal WAT at 5 weeks after HFD feeding (Fig. 1A). Interestingly, staining the adipose tissue sections with 520 MMP FRET Substrate, which becomes fluorescent upon cleavage, revealed increased MMP activity after HFD feeding, and the activity was primarily localized in the CLSs (Fig. 1B).

¹Department of Microbiology and Immunology, Brody School of Medicine, East Carolina University, Greenville, NC 27858, USA. ²Department of Biochemistry and Molecular Biology, Brody School of Medicine, East Carolina University, Greenville, NC 27858, USA. ³Department of Biochemistry and Molecular Biophysics, Kansas State University, Manhattan, KS 66506, USA. ⁴Department of Pharmacology, University of Virginia, Charlottesville, VA 22903, USA. ✉email: mehera19@ecu.edu

CLSs within the adipose tissue are comprised of macrophages that adopt a metabolically activated phenotype characterized by increased lysosomal activity and increased expression of pro-inflammatory cytokines, comparable to M1 activation⁷. While pro-inflammatory cytokines have been shown to increase MMP expression, it is unclear what type of gelatinases are produced by M1-like pro-inflammatory macrophages, such as those found in the CLSs⁸. We polarized mouse bone marrow-derived macrophages to M1 (pro-inflammatory) or M2 (anti-inflammatory) and analyzed the MMPs produced in the supernatant with a gelatin zymogram and western blot. Interestingly, M0 (unpolarized), M1, and M2 macrophages all produced MMP9 while only M2 macrophages produced MMP2 (Fig. 1C and Sup. Figure 2A). To confirm the in vitro results, we examined MMP activity in the gonadal WAT lysate from mice on an NCD or HFD for 16 weeks and surprisingly, only MMP2 activity was detected in the adipose tissue after HFD feeding (Fig. 1D). To determine if other gelatinases such as MMP9 were active in the earlier time points of HFD feeding, we performed zymography of gonadal WAT lysate of mice on HFD for 5–11 weeks and found only MMP2 activity which appeared as early as 5 weeks after HFD (Sup. Figure 1G). Immunohistochemistry staining of gonadal WAT showed increased MMP2 expression around the CLSs in the HFD-fed mice compared to the NCD controls (Fig. 1E). These results suggest that MMP2 is the highly active gelatinase present in the gonadal WAT that localizes to CLSs after HFD-induced obesity.

MMP2 impairs glucose uptake and decreases the glycolytic capacity of 3T3-L1 adipocytes

MMP2 has been previously shown to be secreted by the adipose tissue, and elevated MMP2 plasma levels can be found in obese patients; however, it remains unclear if MMP2 is having effects within the adipose tissue unrelated to its role in extracellular matrix remodeling⁹. Therefore, we treated 3T3-L1 adipocytes with varying physiologically relevant concentrations of recombinant mouse MMP2^{5,6} and performed a glycolysis stress test in a Seahorse XFe24 Extracellular Flux Analyzer. The MMP2 protein was supplied as an inactive form and was activated by using 1 mM p-Aminophenylmercuric acetate (APMA), which was confirmed by generation of a lower molecular weight MMP2 via a Western blot (Sup. Figure 3A). Before treating the adipocyte with activated MMP2, we confirmed its activity at 200, 400, and 800 ng/ml (corresponds 2.5, 5, and 10 nM, respectively) to using the 520 MMP FRET Substrate (Sup. Figure 3B). Finally, we treated the starved (cultured for 2 h with 5 mM D-Glucose without serum) adipocytes with or without 400 nM insulin (final concentration) with or without MMP2 at 200, 400, or 800 ng/ml (final concentration), and determined extracellular acidification rate (ECAR) in real time. During the entire assay, the adipocytes were at least 5 mM glucose. As expected, treatment with insulin alone significantly increased glycolysis, glycolytic capacity, and the glycolytic reserve of the adipocytes (Fig. 2A). However, the presence of 400 and 800 ng/ml MMP2 significantly attenuated insulin-stimulated increased glycolysis, glycolytic capacity, and the glycolytic reserve (Fig. 2A). Furthermore, treatment with a specific MMP2 inhibitor which blocks MMP2's catalytic activity (Fig. 2B), rescued glycolytic parameters (Fig. 2C). Microscopy images of the cells before and after treatment for 40 min with varying concentration of MMP2, and further incubation in a non-CO₂ incubator for 3 h did not show evidence of detachment, suggesting this effect of MMP2 is not due to cell loss as a result of extracellular matrix degradation (Sup Fig. 4A).

To determine if decreased glycolysis was because of decreased glucose uptake, we examined glucose uptake in 3T3-L1 adipocytes via flow cytometry of live adipocytes (Fig. 3A) after treatment with varying concentrations of MMP2 (Fig. 3B). In agreement with the results from the glycolysis stress test, glucose uptake was significantly decreased after treatment with 400 or 800 ng/mL of MMP2 (Fig. 3B) and reduced glucose uptake at 400 ng/ml of MMP2 was reversed after treatment with the MMP2 inhibitor (Fig. 3C). Analysis of the percent of live cells (DAPI negative) showed that up to 800 ng/mL of MMP2 treatment for 30 min did not cause significant cell death, suggesting that the levels of MMP2 used were well tolerated by the 3T3-L1 adipocytes for the time they were exposed to (Sup. Figure 4B).

As degradation of insulin by MMP2 may result in reduced glycolysis and glucose uptake, we tested MMP2 cleavage of recombinant insulin up to 20 h. As a positive control, gelatin at the same micromolar concentration was incubated with MMP2. Coomassie staining failed to show any cleavage products of inulin after incubation with MMP2, while gelatin showed significant degradation (Sup Fig. 4C). Binding of insulin to MMP2 may affect insulin activity. However, analysis of a mixture of inulin and MMP2 via size exclusion chromatography did not show binding of insulin with MMP2 (Sup Fig. 4D). Altogether, these results suggest that MMP2, via protease activity or by binding to the extracellular domain of GLUT4, impairs cellular glucose uptake leading to decreased glycolysis.

The extracellular domain of the GLUT4 receptor contains a putative MMP2 cleavage site

Insulin-dependent glucose influx by 3T3-L1 adipocytes largely relies on cell surface GLUT4¹⁰. Amino acid sequence analysis of GLUT-4 identified an extracellular loop between the first and second helices that contains a putative MMP2 cleavage motif PXXXHy¹¹. XHy represents a large hydrophobic residue in the P1' position; in GLUT4 it is isoleucine. AlphaFold2 (AF2) in silico folding analysis utilizing murine GLUT4 extracellular loop (Uniprot: P14142, residues 64–77) and full-length murine MMP2 (Uniprot: P33434), conformed the peptide to the active site of MMP2 in a substrate-like fashion with isoleucine occupying the P1' pocket adjacent to the catalytic glutamine (Fig. 4A). To verify the in silico prediction, we created a GLUT4 loop peptide (residues 63–77) and performed an enzymatic competition assay with the 520 MMP FRET Substrate. The addition of the GLUT4 loop peptide and a positive control peptide, but not the negative control peptide (the GLUT4 loop peptide in reverse order), significantly decreased the fluorescent signal (Fig. 4B). This indicates the GLUT4 loop peptide, at least, binds to the substrate binding site of MMP2 and reduces its ability to cleave the substrate.

To determine if MMP2 cleaves the GLUT4 loop peptide, we incubated a mixture of MMP2 with GLUT4 loop peptide, the reverse GLUT4 loop peptide (negative control) and an MMP substrate peptide at 37 °C for 18 h and analyzed the mixtures using size exclusion chromatography (Fig. 4C). Peptides at 20 μM were detected at UV absorbance 214 nM, but not at 280 nM. MMP2, even at 800 ng/ml (10 nM), was below the detection limit

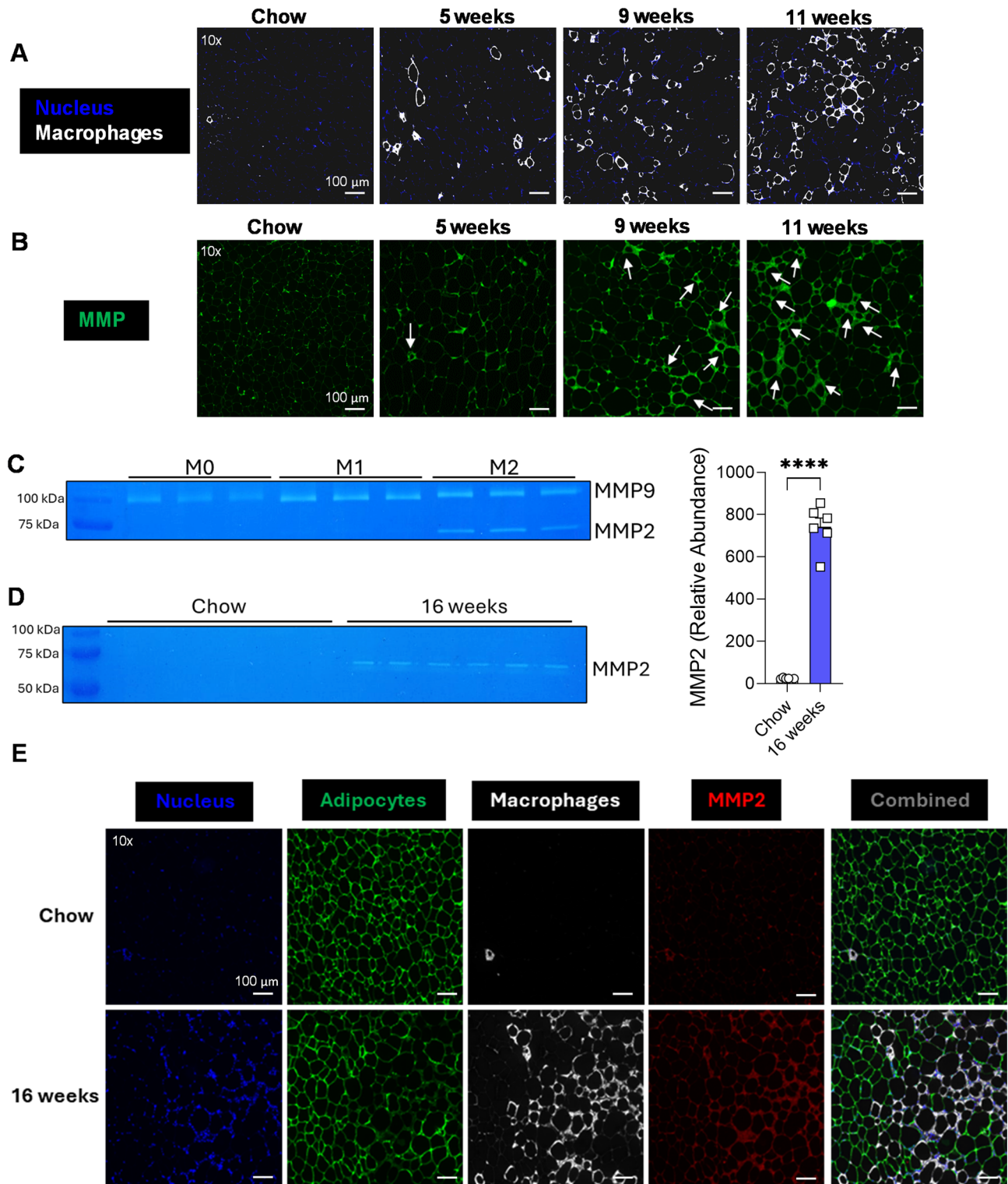


Fig. 1. MMP2 is the highly active gelatinase in white adipose tissue during obesity. (A) Representative confocal images of gonadal WAT from mice on HFD for 5, 9, or 11 weeks or NCD (Chow) for 11 weeks stained for nucleus (DAPI-blue), macrophages (Mac2-white). (B) Representative images of gonadal WAT from HFD for 5, 9, or 11 weeks or NCD for 11 weeks stained with MMP FRET Substrate (green). (C) Gelatin zymogram of culture supernatant from M0 (unpolarized), M1 (pro-inflammatory), and M2 (anti-inflammatory). (D) Gelatin zymogram and relative abundance of MMP2 in gonadal WAT lysate from mice on HFD or NCD for 16 weeks. (E) Representative images of gonadal WAT from mice on HFD or NCD for 16 weeks stained for nucleus (DAPI-blue), adipocytes (FABP4-green), macrophages (Mac2-white), MMP2 (red). Values are expressed as means \pm SEM. $^{****}, p < 0.0001$ by parametric unpaired t-test. $n = 4$ mice, 1 section per mouse, 3–4 images per section (A,B), $n = 3$ (C), $n = 6$ (D), $n = 6$ mice, 1 section per mouse, 3–4 images per section (E). Scale bars: 100 μ m (A,B,E).

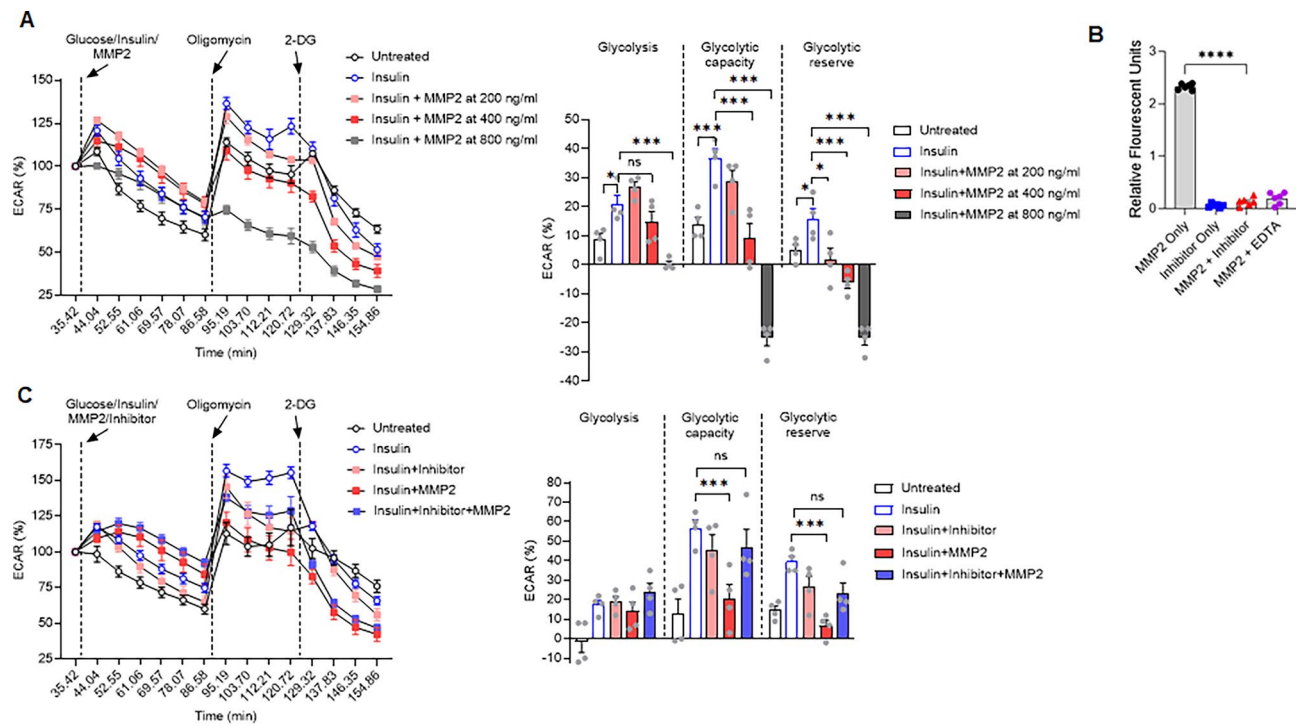


Fig. 2. MMP2 decreases glycolysis in 3T3-L1 adipocytes. **(A)** Aerobic glycolysis of adipocytes after treatment with 400 nM insulin without or with 200 ng/mL, 400 ng/mL, or 800 ng/mL of active MMP2 (ECAR, extracellular acidification rate). **(B)** MMP substrate cleavage assay: MMP FRET Substrate which becomes fluorescent after cleavage, was incubated with 400 ng/ml (5 nM) MMP2, MMP2 inhibitor I only (1 μ M), MMP2 with MMP2 inhibitor I, or MMP2 with 50 mM EDTA. **(C)** Aerobic glycolysis of adipocytes after treatment with insulin with 400 ng/mL (5 nM) of active MMP2, MMP2 inhibitor I (1 μ M), or MMP2 with MMP2 inhibitor I. Values are expressed as means \pm SEM. *, $p < 0.05$; **, $p < 0.01$; ***, $p > 0.001$, ****, $p < 0.0001$ two-way ANOVA with Tukey's multiple comparison test. $n = 4$ from single experiment (A,C) and $n = 6$ (B).

of the UPLC. MMP2 cleaved the MMP substrate peptide resulting in two smaller molecular weight fragments. No smaller peptide fragments were identified in the MMP2 and GLUT4 loop peptide or the reverse peptide, however, a broad peak was noticeable for the MMP2 and GLUT4 loop peptide mixture suggesting, at least, MMP2 binds to the GLUT4 loop peptide (Fig. 4C).

Sequence alignment between murine and human GLUT4 shows a high identity between the extracellular loops of both proteins (Fig. 4D), suggesting that the MMP2 binding or cleavage of GLUT4 may be conserved among mice and humans. Furthermore, the sequence alignment of murine and human GLUT1 and GLUT3 to GLUT4 showed low identity (Fig. 4D), especially surrounding the proposed GLUT4 cleavage site, indicating that the cleavage event may be specific to GLUT4. Altogether, these results suggest that mouse GLUT4 has a potential MMP2 binding site, that is conserved in human GLUT4.

Discussion

Here, we show that MMP expression is increased in the gonadal WAT of IR mice, and the increased MMP expression is concentrated around CLSs. Furthermore, MMP2 is the highly active gelatinase in the gonadal WAT of HFD-fed obese mice. MMP2 treatment impaired glucose uptake and aerobic glycolysis in 3T3-L1 adipocytes, and inhibition of MMP2 activity reversed the impairment in metabolism. In silico structural analysis identified a putative MMP2 cleavage site on an extracellular domain of both murine and human. The GLUT4 extracellular domain was confirmed as it binds to the MMP2.

Future studies are needed to determine the if MMP2 cleaves the cell surface loop of GLUT4. We hypothesize that cleavage of the GLUT4 at the proposed site would ablate the ability of GLUT4 to transport glucose across the cell membrane. The process of GLUT4 facilitating glucose across the membrane requires multiple conformational changes of the GLUT4 protein, which would no longer be possible once the protein is cleaved^{12,13}. It is also possible that the MMP2 could sterically inhibit glucose from entering GLUT4 while bound, though the effect would most likely be transient as MMP2 dissociates after cleaving GLUT4. Once cleaved, we hypothesize that the cleaved remnants would be directed to be degraded by the lysosome. GLUT4 is recycled between the plasma membrane and GLUT-containing vesicles¹⁴, and over time, cleavage of the GLUT4 by MMP2 may potentially impact the pool of available GLUT4 as the cell's ability to utilize the recycled GLUT4 is impaired.

MMP2 has been reported to degrade other cell surface receptors found on adipocytes, most notably the leptin receptor¹⁵. Mazor et al. determined that the leptin receptor is a substrate for MMP2 within hypothalamic tissue; further studies are needed to determine how MMP2 degradation of the leptin receptor may affect adipocyte

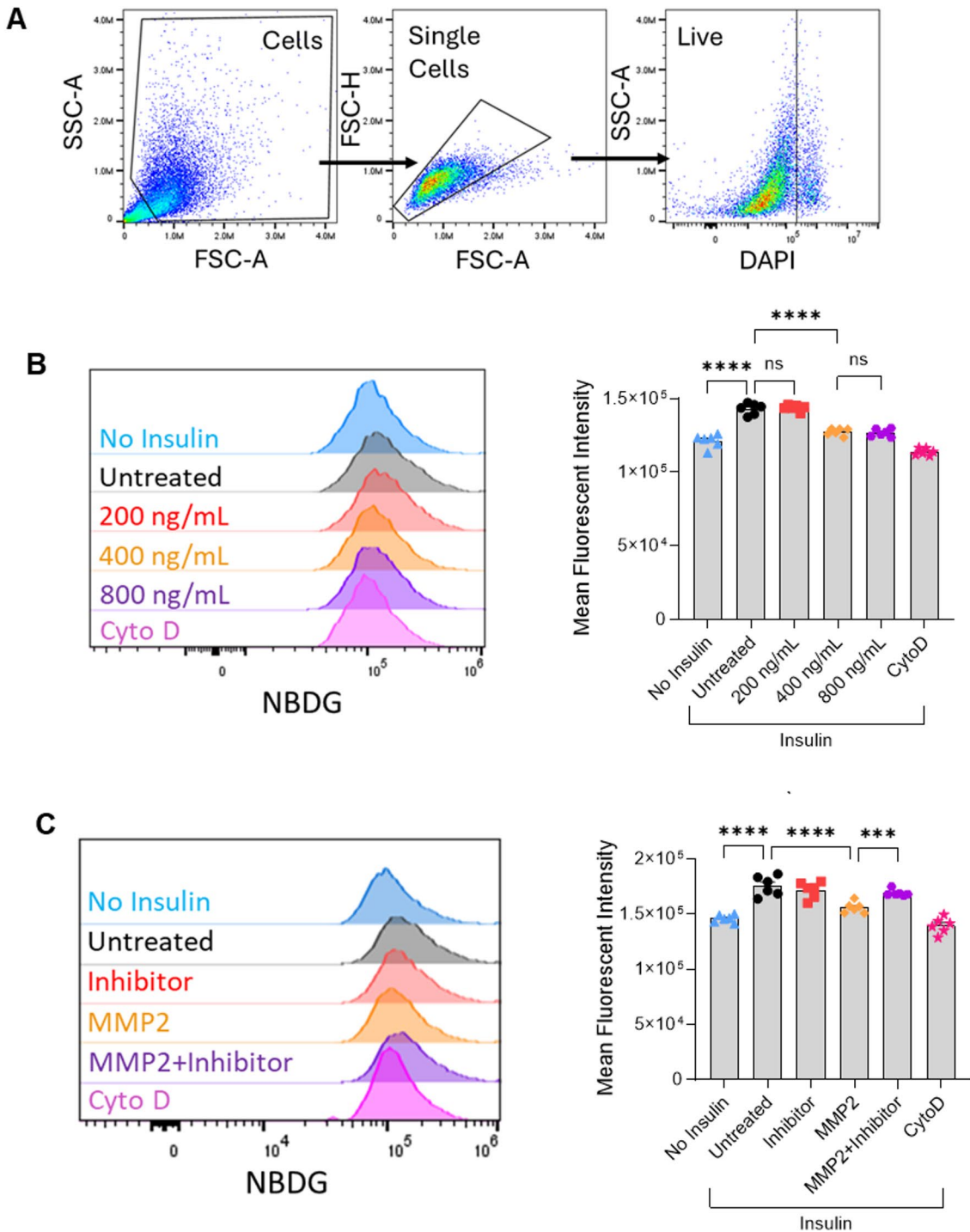


Fig. 3. MMP2 decreases insulin-stimulated glucose uptake in 3T3-L1 adipocytes. (A) Flow cytometry gating for adipocytes in glucose uptake assay. Live adipocytes were used to determine glucose uptake as shown in (B,C). (B) Left panel shows the histograms of 2-NBDG fluorescence of live adipocytes after treatment with 200 ng/mL, 400 ng/mL, or 800 ng/mL of MMP2 and right panel shows the quantification of mean fluorescence intensity (MFI). As a negative control of glucose uptake, some cells were pretreated with Cytochalasin D (10 μ M, CytoD) for 1 h. (C) Left panel shows the histograms of 2-NBDG of live adipocytes after treatment with 400 ng/mL (5 nM) of MMP2, MMP2 inhibitor I (1 μ M), or MMP2 with MMP2 inhibitor I and right panel shows the quantification of MFI. Values are expressed as means \pm SEM. ***, $p < 0.001$, ****, $p < 0.0001$ by one-way ANOVA with Tukey's multiple comparison test. $n = 6$ (A–C)

Figure 4

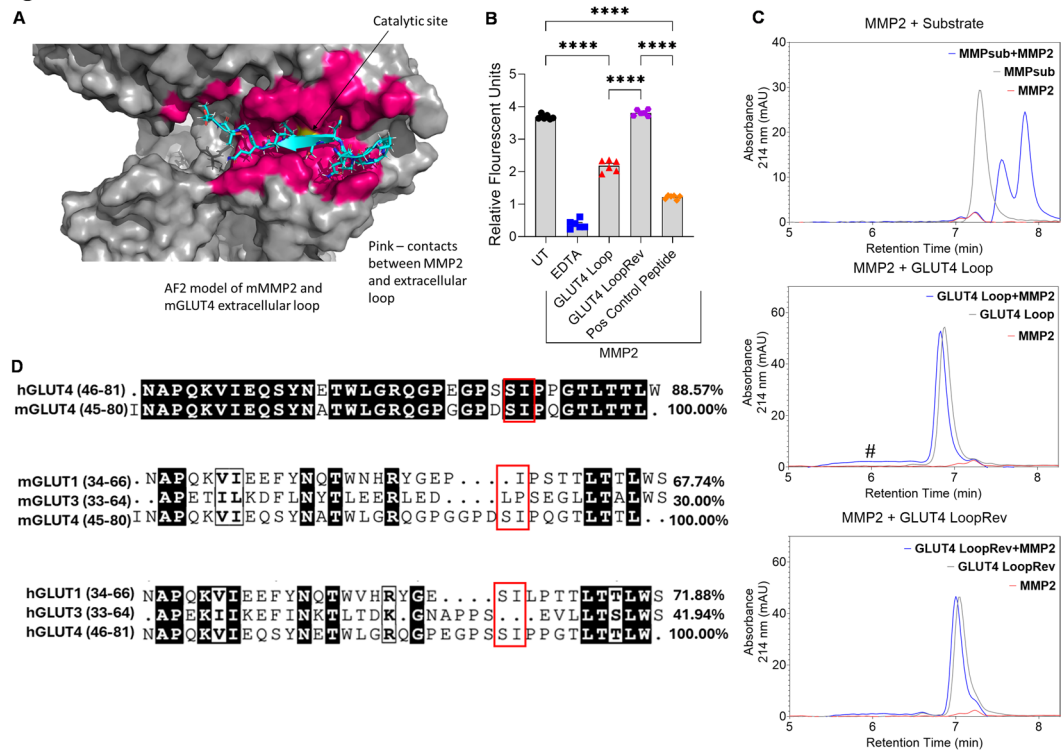


Fig. 4. A putative MMP2 cleavage site is localized in an extracellular domain of the GLUT4 receptor. (A) AlphaFold model of interaction between murine MMP2 and murine GLUT4 extracellular loop (residues 64–77). Pink represents contacts between MMP2 and the extracellular loop. (B) MMP FRET Substrate cleavage competition assay: MMP FRET Substrate was incubated at 37 °C with 5 nM MMP2 alone or MMP2 with 50 mM EDTA, 500 μM GLUT4 loop peptide, 500 μM negative control peptide (GLUT4 LoopRev), or 500 μM positive control peptide. After 30 min, fluorescent intensity of the reactions was determined using a plate reader. (C) Size exclusion chromatography of peptide and MMP2 mixtures: an MMP substrate peptide (MMPsub), GLUT4 loop peptide (GLUT4 Loop), or the reverse peptide (GLUT4 LoopRev) at 20 μM was incubated with 10 nM MMP2 for 18 h at 37 °C and analyzed using a size exclusion chromatography column. The amide bonds in the peptides were detected using UV absorbance 214 nm. '#' indicates the broad peak for MMP2-peptide complex. (D) Sequence alignment of the extracellular loop between the first and second helix of human GLUT4 and murine GLUT4; murine GLUT1, murine GLUT3, and murine GLUT4; and human GLUT1, human GLUT3, and human GLUT4. Red box indicates MMP2 cleavage site. Values are expressed as means + SEM. ****, $p < 0.0001$ by one-way ANOVA with Tukey's multiple comparison test. $n = 6$ (B).

function in vivo. While 3T3-L1 adipocytes differentiated with Isobutylmethylxanthine/Dexamethasone/Insulin, as we did in our study, do express the leptin receptor, leptin mRNA and leptin secretion by the cells is very low¹⁶; therefore, cleavage of the leptin receptor would not significantly impact the glucose uptake and glycolysis of the cells. Future studies utilizing an alternative adipocyte differentiation protocol¹⁶ or the addition of exogenous leptin to understand the interplay between GLUT4 and leptin receptor cleavage in the context of adipocyte metabolism would be warranted.

Apart from its role in matrix remodeling, MMP2 can precisely process the chemokine stromal cell-derived factor-α to a neurotoxin protein that promotes neuronal apoptosis and neurodegeneration¹⁷. MMP2 can be activated by the disruption of the cysteine-Zn²⁺ bond, either by proteolysis to an enzymatically active form¹⁸ or by conformational changes caused by reactive oxygen-nitrogen species (RONS)¹⁹. Proteolysis of MMP2 is facilitated by the formation of a trimeric complex of MMP2, tissue inhibitors of metalloproteinase 2 (TIMP2), and membrane-type 1 MMP (MT1-MMP or MMP-14) on the cell surface²⁰. Both TIMP2 and MT1-MMP are upregulated in obese adipose tissue, and adipocyte-specific overexpression of MT1-MMP in obese mice impairs lipid metabolism and insulin resistance^{21,22}. Furthermore, RONS are increased in obese adipose tissue and produced by pro-inflammatory macrophages in CLSs^{23,24}. Here we demonstrate increased MMP activity and MMP2 expression in CLSs, suggesting that RONS produced by the pro-inflammatory macrophages may be one of the primary activators of MMP2 during obesity.

MMP2 has also been identified as a regulator of adipocyte differentiation. Treatment of 3T3-L1 fibroblasts with a specific MMP2 inhibitor impairs adipogenic differentiation, primarily in the early stages of differentiation²⁵. Genetically *Mmp2* deficient mice are leaner and exhibit lower weight and growth rates at birth²⁶. Furthermore, *Mmp2* deficiency causes less fat accumulation in mice when challenged with an HFD²⁷. It remains unclear

through what mechanism MMP2 promotes adipocyte differentiation. Due to MMP2's effect on adipocyte differentiation, our studies utilized fully differentiated 3T3-L1 adipocytes before treatment with MMP2.

Our studies focus on the effect of MMP2 on glucose utilization and adipocyte metabolism using 3T3-L1 adipocytes as an in vitro model of white adipocytes. As in vitro models cannot fully recapitulate the complexities of in vivo physiology, future studies on mouse models are required to fully delineate the effect of MMP2 on adipocyte glucose metabolism during obesity. As genetic deletion of *Mmp2* results in mice with low body weight and defects in growth rate, utilization of a global inducible *Mmp2*-floxed mouse model is necessary to determine the physiological role of MMP2 on the development of insulin resistance and hyperglycemia.

Altogether, our study shows a novel function of MMP2, which may contribute to hyperglycemia during obesity. Furthermore, GLUT4 is expressed in aortic smooth muscle cells and reduction of GLUT4 levels in the aorta has been linked to hypertension and aortic dissection during metabolic disease^{28,29}. This suggests that MMP2 may be a therapeutic target of interest to enhance glucose utilization in patients with a variety of metabolic and cardiovascular diseases.

Methods

Mice

Eight-week-old male C57BL/6J mice (#380050, Jackson Laboratory, Bar Harbor, ME) were given water and fed a high-fat diet (HFD, #F3282, Bio-Serv; 60% of calories from fat) for 5 to 16 weeks or with a normal chow diet (NCD, Prolab IsoPro RMH 3000 5P76, LabDiet) for 11 or 16 weeks. The mice were euthanized with 100% carbon dioxide and sacrificed by cervical dislocation in accordance with the 2013 edition of American Veterinary Medical Association guidelines for the euthanasia of animals. All protocols involving animals were approved by the East Carolina University Animal Care and Use Committee and performed in an AAALAC-accredited facility in accordance with current NIH guidelines. This study is reported in accordance with ARRIVE guidelines.

Isolation of SVF from adipose tissue

The left and the right gonadal white adipose tissue (WAT) was excised from the mouse and one of the fat pads was used for the isolation of the stromal vascular fraction (SVF). The tissue was minced with scissors and digested for 1 h in Hanks Balanced Salt Solution (HBSS, Gibco) with 2% bovine serum albumin (BSA) and 2 mg/ml of collagenase type I shaking at 37 °C. After digestion, tissue was filtered through a 500 µm nylon mesh strainer and washed with HBSS with 2% BSA. The cells were centrifuged (450×g for 5 min) to allow the stromal vascular fraction (SVF) to separate the adipocytes floating on the top of the buffer. The SVF pellet was collected, and red blood cells were lysed. Cells were washed, centrifuged, and resuspended in various buffers depending on downstream use.

Flow cytometry

The SVF from WAT was isolated as described above. The cells were blocked with purified anti-mouse CD16/32 (BioLegend, San Diego, CA; #101302) and stained with the following fluorescent conjugated antibodies from BioLegends and FisherScientific for 30 min on ice: PE Cyanine7 anti-F4/80 (#25-4801-82), Brilliant Blue 515 anti-CD45 (#564590), and APC anti-CD11b (#17-0112-83), Brilliant Violet 711 anti-CD206 (#141727), and Brilliant Violet 605 anti-CD86 (#105037). Invitrogen DAPI (4',6-diamidino-2-phenylindole, dihydrochloride) (#D1306) was used for staining the dead cell. The samples were run on the flow cytometer machine Cytek Biosciences Cytek Aurora, USA. Data analysis and quantification were performed using FlowJo v10.6.2.

Plasma insulin quantification

Fasting plasma insulin levels were measured with an Ultra-Sensitive Mouse Insulin ELISA Kit (Crystal Chem, Elk Grove Village, IL; # 90080) per manufacturer instructions.

Western blot

Adipose tissue was homogenized in a bead mill with TPER buffer (ThermoFisher Scientific #78510) containing a protease inhibitor cocktail (Sigma-Aldrich). For Analysis of macrophage supernatant, bone-marrow-derived macrophages were induced to either M1 or M2 or left uninduced (M0) as described below. Macrophages were cultured overnight in RPMI 1640 media (without serum) and cell culture supernatant was collected. 50 µl of the culture supernatants were resolved in a 4–12% Tris-Glycine SDS-PAGE (under reducing conditions), and MMP2 and MMP9 proteins were detected after Western blotting. To verify activation of MMP2, 50 µg/mL of MMP2 was incubated with 1 mM N-(3-Aminopropyl)methacrylamide hydrochloride (APMA) (Sigma Aldrich, #731099) in reaction buffer (50 mM Tris-HCl pH 7.5, 10 mM CaCl₂, 150 mM NaCl, 5 µM ZnCl₂) at 37 °C for varying timepoints. The protein was analyzed using 4–12% Tris-Glycine SDS-PAGE, followed by a Western blot against an MMP2 antibody. The primary antibodies used are anti-AKT (Cell Signaling Technologies, #9271), anti-pAKT Ser473 (Cell Signaling Technologies, #4060s), anti-MMP2 (Proteintech, #10373-2-AP), and anti-MMP9 (Cell Signaling Technology, #24317) and the IRDye-conjugated secondary antibodies were from LI-COR. The blots were detected, and band intensities were quantified using LI-COR's Image Studio software version 5.2.5.

SDS-PAGE to determine MMP2 activity on insulin and gelatin

5 nM of activated MMP2 (BioLegend, #554402) was incubated with 20 µM of insulin (Humulin R) or 125 µg/mL of gelatin (Sigma Aldrich, #G1890) at 37 °C for 0 min, 30 min, 1 h, 2 h, or 20 h. The samples were analyzed using 4–12% Tris-Glycine SDS-PAGE.

Real-time qPCR

Stromal vascular fraction from the gonadal white adipose tissue was isolated as described above and resuspended in TRIzol reagent (ThermoFisher, # 15596026) and RNA fraction was isolated per manufacturer's instructions. RNA was purified with RNeasy Mini Kit (Qiagen, # 74104) per manufacturer's instructions. cDNA was synthesized and real-time PCR was performed on a CFX Connect™ Real-Time PCR Detection System as described previously^{30,31}. The abundance of *B2m* mRNA was used for relative quantification of *Tnfα* mRNAs in the SVF.

Immunohistochemistry

Five-micrometer gonadal WAT cross-sections were hydrated with HistoClear Clearing Agent (MilliporeSigma), 100% ethanol, 90% ethanol, 70% ethanol, 20% ethanol, and then water. Antigen retrieval was performed by boiling the slides in the Antigen Unmasking Solution (Vector Laboratories, Burlingame, CA; #H-3300). After antigen retrieval, the sections were treated with 10% donkey serum and incubated with primary Ab for 14–16 h at 4 °C. Primary antibodies were detected by fluorescent secondary antibodies. The slides were mounted with ProLong Gold Antifade Mountant with DAPI (Invitrogen, #P36931) before image acquisition on a Laxco LMI 6000 Series Inverted microscope (Fisher Scientific) or EVOS M5000 (ThermoFisher). The primary antibodies used were anti-FABP4/A-FABP (Novus Biologics; #AF1443), anti-Mac-2 (Cederlane; #CL8942AP), anti-MMP2 (ThermoFisher, #10373-AP) antibody. The secondary antibodies used are Donkey anti-Goat Alexa Fluor Plus 488 (ThermoFisher; #A32814), Donkey anti-Rabbit Alexa Fluor Plus 555 (ThermoFisher; #A32794), and Donkey anti-Rat Alexa Fluor Plus 647 (ThermoFisher; A48272).

In situ zymography was performed on fixed five-micrometer gonadal WAT cross-sections hydrated with HistoClear Clearing Agent (MilliporeSigma), 100% ethanol, 90% ethanol, 70% ethanol, 20% ethanol, and then water³². Sections were then incubated with 520 MMP FRET Substrate (Anaspec, #AS-60568-01) in reaction buffer (50 mM Tris-HCl pH 7.5, 10 mM CaCl₂, 150 mM NaCl, 5 μM ZnCl₂) at 37 °C in dark overnight. The slides were mounted with ProLong Gold Antifade Mountant with DAPI (Invitrogen, #P36931) before image acquisition on a EVOS M5000 (ThermoFisher).

Gelatin zymogram

Adipose tissue was homogenized in a bead mill with TPER buffer (ThermoFisher Scientific #78510) containing a protease inhibitor cocktail (Sigma-Aldrich). Protein concentration was determined by Pierce BCA protein assay (ThermoFisher Scientific, #23227). Alternatively, bone marrow-derived macrophages were induced to either M1 or M2 or left uninduced (M0) as described below. Macrophages were cultured overnight in RPMI 1640 media (without serum) and 15 μl of the cell culture supernatant was used for zymography. Non-reduced total lysate of adipose tissue was loaded at a concentration of 15 μg/mL onto a 12% SDS-polyacrylamide gel containing 1 mg/mL of porcine gelatin (Sigma Aldrich, #G1890). Following electrophoresis, the gels were washed and renatured with washing buffer (2.5% Triton X-100, 50 mM Tris-HCl pH7.5, 5 mM CaCl₂, 1 μM ZnCl₂) with two 30 min washes at room temperature. Gels were then incubated with substrate buffer (1% Triton X-100, 50 mM Tris-HCl pH 7.5, 5 mM CaCl₂, 1 μM ZnCl₂) at 37 °C for 24 h. Gels were stained with Coomassie Blue staining solution (40% Methanol, 10% Acetic Acid, 0.5% Coomassie Blue) for 30 min at room temperature and then destained with destaining solution (40% Methanol, 10% Acetic Acid) for 1 h. Band intensities were quantified using LI-COR's Image Studio software version 5.2.5.

Preparation of bone marrow-derived macrophages and differentiation of 3T3-L1 adipocytes

The bone marrow-derived macrophages and 3T3-L1 adipocytes were prepared as described before³⁰. Briefly, bone marrow cells from the femur and tibia of C57BL6/J mice were collected, red blood cells were lysed with lysis buffer and the cells were cultured at a density of 1 to 2 × 10⁶ cells/mL in RPMI 1640 medium containing 10% FBS (Gibco Fetal bovine serum, ThermoFisher, #1600-044, heat-inactivated) and 1% antimycotic-antibiotic (Thermo-Fisher, #15240-062), supplemented with 20% L929 (NCTC clone 929; ATCC, Manassas, VA) culture supernatant. The culture medium was changed on the fourth day and then on every second day. On day 8 of differentiation, M1 or M2 macrophages were induced by incubation with 1 μg/mL of LPS and 50 ng/mL of IFNγ or 20 ng/mL of IL-4, respectively, for 24 hours at 37 °C.

3T3-L1 fibroblasts were cultured in DMEM supplemented with 10% heat-inactivated (HI) FBS at 37 °C, 95% relative humidity, and 5% CO₂. For differentiation into adipocytes, cells were grown to confluence and treated for 4 days with differentiation media containing DMEM, 10% HI FBS, 1x antibiotic-antimycotic, 0.25 U/mL insulin (Humulin R, Lilly), 0.5 mM 3-isobutyl-1-methylxanthine, 0.025 mM dexamethasone, and, on day 5, cells were treated with post-differentiation media containing DMEM, 10% HI FBS, 0.25 U/mL insulin and then adipocytes were maintained in DMEM with 10% heat-inactivated FBS. 3T3-L1 adipocytes were used in glucose uptake and seahorse experiments on day 6 of differentiation.

Glucose uptake

3T3-L1 adipocytes, 5 days after differentiation, were seeded 1 day prior to glucose uptake assay on 24-well plates coated with Poly-L-lysine solution (P4832, Sigma-Aldrich, USA) and incubated overnight at 37 °C to adhere. Cells were washed with phosphate buffered saline (PBS) and incubated for 2 h in low glucose DMEM (Sigma, #D5030; 5 mM D-glucose, Sigma, #G7021; 4 mM Gibco L-Glutamine, ThermoFisher, #A2916801, pH 7.4). For the MMP2 concentration titration assay, cells were left untreated or treated with 200 nM insulin (Humulin R, Lilly) plus 200, 400, or 800 ng/mL of activated MMP2 (2.5 nM, 5 nM, and 10 nM of MMP2 respectively) (Biologen, #55402) in low Glucose DMEM for 20 min at 37 °C. For the MMP2 inhibitor assay, cells were left untreated or treated with 200 nM insulin with 400 ng/mL active MMP2, 1 μM MMP2 inhibitor I (Cayman chemicals, #19644), or active MMP2 with MMP2 inhibitor in low glucose DMEM for 20 min at

37 °C. Cells were then treated with 200 µg/mL 2-NBDG (2-(N-(7-Nitrobenz-2-oxa-1,3-diazol-4-yl)Amino)-2-Deoxyglucose) (Thermofisher, #N13195) for 10 min at 37 °C. After incubation, cells were washed, removed with accutase (StemCell Technologies), and glucose uptake was analyzed by flow cytometer. Cells were pretreated with Cytochalasin D (10 µM; Cayman Chemicals) after 1 h as a negative control for glucose uptake.

Seahorse extracellular flux assays

3T3-L1 fibroblasts (ATCC, #CL-173) at a density of 2×10^5 /well in DMEM high glucose (DMEM 1X, Corning, #10-013-CM) with 10% FBS (Gibco Fetal bovine serum, ThermoFisher, #1600-044, heat-inactivated) and 1% anti-anti (Thermo-Fisher, #15240-062) seeded on XFe24 well microplates coated with Poly-L-lysine solution (P4832, Sigma-Aldrich, USA). This cell density confluent the wells to 100%. After 4 days of culture to arrest any cell division, the cells were differentiated into adipocytes as described earlier³³ and used for the assay on day 6–8 of differentiation. Before the assay, the cells were washed with 1x PBS and starved for 2 h with low glucose DMEM (Sigma, #D5030; 5 mM D-glucose, Sigma, #G7021; 4 mM Gibco L-Glutamine, ThermoFisher, #A2916801, pH 7.4), and maintained with the same medium throughout the assay. Following starvation, the cells were incubated in a non-CO₂ chamber for 30 min, and then loaded in the Seahorse XFe24 Extracellular Flux Analyzer and a glycolysis stress test was performed as described before³⁴. Briefly, each well in the in the microplate contained 450 µl of the low glucose medium, and the port A of the sensor cartridge contained 50 µl of 10x D-glucose with/without insulin, various concentrations of MMP2, or the MMP2 inhibitor I, port B with 56 µl Oligomycin A (Sigma, #A8674), and port C with 62 µl of 2-Deoxy-D-glucose (Sigma-Aldrich, #D6134). The glycolysis stress test was performed with initial 4 readings of extracellular acidification rate or ECAR to detect basal glycolysis, then contents of port A were injected, and 6 readings were recorded, followed by injection of port B (Oligomycin A) with 4 readings, and port C (2-Deoxy-D-glucose) with 4 readings. During the assay, the final concentrations were: D-glucose, 40 mM; insulin (Humulin R, Lilly), 400 nM; MMP2 at 200, 400, or 800 ng/ml; inhibitor I at 1 µM; Oligomycin at 10 µM; and 2-Deoxy-D-glucose at 80 mM. The assay was performed with $n=4$ per group and was repeated at least 2 times. Since the basal glycolysis, that is, initial ECR readings before the injection of D-glucose were different for each well, the last reading before injection of D-glucose was normalized to 100%. The data were analyzed using Wave 2.6.3 and the rate of glycolysis after injection of D-glucose, the glycolytic capacity of the cells, and the glycolytic reserve were calculated as described before³⁴ using Excel and GraphPad Prism.

MMP substrate cleavage assay

In black 96-well plate 2.5 nM (200 ng/mL), 5 nM (400 ng/mL), or 10 nM (800 ng/mL) of MMP2 (BioLegend, #554402) were incubated with 5 µM of 520 MMP FRET Substrate (Anaspec, #AS-60568-01) in MMP substrate buffer (50 mM Tris-HCl pH 7.5, 10 mM CaCl₂, 150 mM NaCl, 5 µM ZnCl₂). Fluorescence was measured at 37 °C for 120 min on Varioskan LUX (ThermoFisher) at 494/521 excitation/emission.

For verification of MMP2 inhibitor, 5 nM (400 ng/mL) of MMP2, 1 µM of MMP2 inhibitor (Cayman Chemicals, #19644), 5 nM of MMP2 with 1 µM of MMP2 inhibitor, or 5 nM of MMP2 with 50 mM EDTA as negative control were incubated with 5 µM of 520 MMP FRET Substrate (AnaSpec) for 30 min at 37 °C in MMP substrate buffer.

For the substrate competition assay, 5 nM of MMP2 with 500 µM of GLUT4 loop peptide (RQGPGGPDSIPQGTL, GenScript), 500 µM of negative control peptide (LTGQPISDPGGPGQR, GenScript, reverse of GLUT4 loop), 500 µM positive control peptide (VPLSLYSG, Bachm, #4109381), or 50 mM EDTA were incubated with 5 µM of 520 MMP FRET Substrate for 30 min in MMP substrate buffer.

Ultra-performance liquid chromatography (UPLC)

The peptide (20 µM)-MMP2 (10 nM) reactions and controls in 25 µl MMP substrate buffer were incubated for 18 h at 37 °C and analyzed using Waters ACQUITY H-Class UPLC with the size exclusion chromatography column ACQUITY Protein BEH SEC Column, 125 Å, 1.7 µm, 4.6 mm x 150 mm. Sample manager and column temperatures were maintained at 20 °C with a flow rate of 0.3 mL/min. In this assay, 10 nM (800 ng/ml) of MMP2 was used so that any interaction with the peptide can be detected via UV absorbance. 10 µL volumes were injected in duplicate and absorbance was monitored at 214 nm and 280 nm by Waters ACQUITY Tunable UV (TUV) Detector. Similarly, 20 µM of insulin (Humulin R, Lilly) alone or was mixed with 10 nM MMP2, incubated at 37 °C for 2 h, and analyzed via UPLC. All samples were analyzed against Waters BEH SEC protein standard mix (Thyroglobulin, IgG, BSA, Myoglobin, Uracil).

Statistical analysis

The data were analyzed by using GraphPad Prism 8 (GraphPad Software, La Jolla, CA) and Excel (Microsoft Corporation, Redmond, WA), and they are presented as means \pm SEM. Differences between the mean values of the two groups were determined by using t-tests. The means of multiple groups were compared by using a one- or two-way analysis of variance (depending on one independent variable or 2 independent variables) and the comparisons were corrected by Tukey's test. The D'Agostino-Pearson normality test was performed on each group. If the *P* value was not significant (> 0.05), a two-tailed parametric test was used; if the *P* value was significant (< 0.05) or if the number of samples was four, a two-tailed nonparametric t-test (U-test) was used to determine significant differences between the groups. In the multiple comparisons, if a significant difference was found among the groups, pairs of groups were compared by using a parametric or nonparametric t-test. Statistical analyses are provided in each figure legend. Differences between the groups were considered significant when $P < 0.05$. *P* values > 0.05 are indicated as 'not significant' or 'ns' in the graphs.

Data availability

All data generated or analyzed during this study are available upon request to Akshaya K. Meher, mehera19@ecu.edu.

Received: 12 December 2024; Accepted: 6 June 2025

Published online: 07 July 2025

References

- Abel, E. D. et al. Adipose-selective targeting of the GLUT4 gene impairs insulin action in muscle and liver. *Nature* **409**, 729–733. <https://doi.org/10.1038/35055575> (2001).
- Albers, P. H. et al. Enhanced insulin signaling in human skeletal muscle and adipose tissue following gastric bypass surgery. *Am. J. Physiol.-Regul. Integr. Comp. Physiol.* **309**, R510–R524. <https://doi.org/10.1152/ajpregu.00228.2014> (2015).
- Pope, B. D., Warren, C. R., Parker, K. K. & Cowan, C. A. Microenvironmental control of adipocyte fate and function. *Trends Cell Biol.* **26**, 745–755. <https://doi.org/10.1016/j.tcb.2016.05.005> (2016).
- Lumeng, C. N., Deyoung, S. M., Bodzin, J. L. & Saltiel, A. R. Increased inflammatory properties of adipose tissue macrophages recruited during diet-induced obesity. *Diabetes* **56**, 16–23. <https://doi.org/10.2337/db06-1076> (2007).
- Boumiza, S. et al. MMPs and tims levels are correlated with anthropometric parameters, blood pressure, and endothelial function in obesity. *Sci. Rep.* <https://doi.org/10.1038/s41598-021-99577-2> (2021).
- Derosa, G. et al. Matrix Metalloproteinase-2 and -9 levels in obese patients. *Endothelium* **15**, 219–224. <https://doi.org/10.1080/10623320802228815> (2008).
- Hill, D. A. et al. Distinct macrophage populations direct inflammatory versus physiological changes in adipose tissue. *Proc. Natl. Acad. Sci.* **115**, E5096–E5105. <https://doi.org/10.1073/pnas.1802611115> (2018).
- Huang, W. C., Sala-Newby, G. B., Susana, A., Johnson, J. L. & Newby, A. C. Classical macrophage activation up-regulates several matrix metalloproteinases through mitogen activated protein kinases and nuclear Factor- κ B. *PLoS ONE* **7**, e42507. <https://doi.org/10.1371/journal.pone.0042507> (2012).
- Lee, Y. J. et al. Serum SPARC and matrix metalloproteinase-2 and metalloproteinase-9 concentrations after bariatric surgery in obese adults. *Obes. Surg.* **24**, 604–610. <https://doi.org/10.1007/s11695-013-1111-z> (2014).
- Yang, J. & Holman, G. D. Comparison of GLUT4 and GLUT1 subcellular trafficking in basal and insulin-stimulated 3T3-L1 cells. *J. Biol. Chem.* **268**, 4600–4603. [https://doi.org/10.1016/S0021-9258\(18\)53438-4](https://doi.org/10.1016/S0021-9258(18)53438-4) (1993).
- Chen, E. I. et al. A unique substrate recognition profile for matrix metalloproteinase-2. *J. Biol. Chem.* **277**, 4485–4491. <https://doi.org/10.1074/jbc.M109469200> (2002).
- Deng, D. et al. Crystal structure of the human glucose transporter GLUT1. *Nature* **510**, 121–125. <https://doi.org/10.1038/nature13306> (2014).
- Yuan, Y. et al. Cryo-EM structure of human glucose transporter GLUT4. *Nat. Commun.* **13**, 2671. <https://doi.org/10.1038/s41467-022-30235-5> (2022).
- Palacios, S., Lalioti, V., Martinez-Arca, S., Chattopadhyay, S. & Sandoval, I. V. Recycling of the Insulin-sensitive glucose transporter GLUT4. *J. Biol. Chem.* **276**, 3371–3383. <https://doi.org/10.1074/jbc.m006739200> (2001).
- Mazor, R. et al. Cleavage of the leptin receptor by matrix metalloproteinase-2 promotes leptin resistance and obesity in mice. *Sci. Transl. Med.* **10**, eaah6324. <https://doi.org/10.1126/scitranslmed.aah6324> (2018).
- Norman, D. et al. ACTH and α -MSH inhibit leptin expression and secretion in 3T3-L1 adipocytes: Model for a central–peripheral melanocortin-leptin pathway. *Mol. Cell. Endocrinol.* **200**, 99–109. [https://doi.org/10.1016/S0303-7207\(02\)00410-0](https://doi.org/10.1016/S0303-7207(02)00410-0) (2003).
- Zhang, K. et al. HIV-induced metalloproteinase processing of the chemokine stromal cell derived factor-1 causes neurodegeneration. *Nat. Neurosci.* **6**, 1064–1071. <https://doi.org/10.1038/nn1127> (2003).
- Cao, J., Sato, H., Takino, T. & Seiki, M. The C-terminal region of membrane type matrix metalloproteinase is a functional transmembrane domain required for Pro-gelatinase A activation. *J. Biol. Chem.* **270**, 801–805. <https://doi.org/10.1074/jbc.270.2.801> (1995).
- Viappiani, S. et al. Activation and modulation of 72 kDa matrix metalloproteinase-2 by peroxynitrite and glutathione. *Biochem. Pharmacol.* **77**, 826–834. <https://doi.org/10.1016/j.bcp.2008.11.004> (2009). <https://doi.org/10.1016/j.bcp.2008.11.004>
- Nagase, H. Cell surface activation of progelatinase A (proMMP-2) and cell migration. *Cell Res.* **8**, 179–186. <https://doi.org/10.1038/cr.1998.18> (1998).
- Nonino, C. B. et al. Differential expression of MMP2 and TIMP2 in peripheral blood mononuclear cells after Roux-en-Y gastric bypass. *Front. Nutr.* <https://doi.org/10.3389/fnut.2021.628759> (2021).
- Li, X. et al. Critical role of matrix metalloproteinase 14 in adipose tissue remodeling during obesity. *Mol. Cell. Biol.* **40**, 1–24. <https://doi.org/10.1128/mcb.00564-19> (2020).
- Politis-Barber, V., Brunetta, H. S., Paglialunga, S., Petrick, H. L. & Holloway, G. P. Long-term, high-fat feeding exacerbates short-term increases in adipose mitochondrial reactive oxygen species, without impairing mitochondrial respiration. *Am. J. Physiol. Endocrinol. Metabol.* **319**, E376–E387. <https://doi.org/10.1152/ajpendo.00028.2020> (2020).
- Nakajima, S. et al. Accumulation of CD11c+CD163+ Adipose tissue macrophages through upregulation of intracellular 11 β -HSD1 in human obesity. *J. Immunol.* **197**, 3735–3745. <https://doi.org/10.4049/jimmunol.1600895> (2016).
- Croissantreau, G., Chrétien, M. & Mbikay, M. Involvement of matrix metalloproteinases in the adipose conversion of 3T3-L1 preadipocytes. *Biochem. J.* **364**, 739–746. <https://doi.org/10.1042/bj20011158> (2002).
- Itoh, T. et al. Unaltered secretion of β -Amyloid precursor protein in gelatinase A (Matrix metalloproteinase 2)-deficient mice. *J. Biol. Chem.* **272**, 22389–22392. <https://doi.org/10.1074/jbc.272.36.22389> (1997).
- Van Hul, M. & Lijnen, H. R. A functional role of gelatinase A in the development of nutritionally induced obesity in mice. *J. Thromb. Haemost.* **6**, 1198–1206. <https://doi.org/10.1111/j.1538-7836.2008.02988.x> (2008).
- Zheng, H. et al. Insulin resistance promotes the formation of aortic dissection by inducing the phenotypic switch of vascular smooth muscle cells. *Front. Cardiovasc. Med.* **8**, 732122. <https://doi.org/10.3389/fcvm.2021.732122> (2021).
- Park, J. L. et al. GLUT4 facilitative glucose transporter specifically and differentially contributes to agonist-induced vascular reactivity in mouse aorta. *Arterioscler. Thromb. Vasc. Biol.* **25**, 1596–1602. <https://doi.org/10.1161/01.ATV.0000170137.41079.ab> (2005).
- Meher, A. K. et al. Nrf2 deficiency in myeloid cells is not sufficient to protect mice from high-fat diet-induced adipose tissue inflammation and insulin resistance. *Free Radic. Biol. Med.* **52**, 1708–1715. <https://doi.org/10.1016/j.freeradbiomed.2012.02.022> (2012).
- Kadl, A. et al. Identification of a novel macrophage phenotype that develops in response to atherogenic phospholipids via Nrf2. *Circ. Res.* **107**, 737–746. <https://doi.org/10.1161/CIRCRESAHA.109.215715> (2010).
- Chen, Z. et al. Gelatin zymography can be performed on fixed brain tissue. *J. Histochem. Cytochem.* **71**, 481–493. <https://doi.org/10.1369/00221554231194118> (2023).
- Lempicki, M. D. et al. BAFF neutralization impairs the autoantibody-mediated clearance of dead adipocytes and aggravates obesity-induced insulin resistance. *Front. Immunol.* **15**, 1436900. <https://doi.org/10.3389/fimmu.2024.1436900> (2024).

34. Lempicki, M. D. et al. BAFF antagonism via the BAFF receptor 3 binding site attenuates BAFF 60-mer-induced classical NF- κ B signaling and metabolic reprogramming of B cells. *Cell. Immunol.* **381**, 104603. <https://doi.org/10.1016/j.cellimm.2022.104603> (2022).

Acknowledgements

We thank Jerald Whitley for technical assistance, East Carolina University Flow Core Facility, Research Histology Core, and Imaging Core for technical support. This project was supported by the Brody School of Medicine at ECU's Mass Spectrometry Core Facilities which has received support from the Golden Leaf Foundation and from federal COVID-19 relief funds appropriated to ECU in North Carolina SL 2020-4.

Author contributions

M.D.L., R.J.G., A.D.H., and A.K.M. designed research; M.D.L., R.J.G., A.D.H., and A.K.M. performed research; T.N.Z., B.L.G., J.C., T.E.H., and A.K.M. contributed new reagents/analytic tools; M.D.L., R.J.G., A.D.H., T.N.Z., and A.K.M. analyzed data; and M.D.L. and A.K.M. wrote the manuscript.

Funding

This work was supported by NIH R01 HL146685 and 2025 Brody Brothers Endowment Grant to A. K. Meher.

Declarations

Competing interests

The authors declare no competing interests.

Additional information

Supplementary Information The online version contains supplementary material available at <https://doi.org/10.1038/s41598-025-06252-x>.

Correspondence and requests for materials should be addressed to A.K.M.

Reprints and permissions information is available at www.nature.com/reprints.

Publisher's note Springer Nature remains neutral with regard to jurisdictional claims in published maps and institutional affiliations.

Open Access This article is licensed under a Creative Commons Attribution-NonCommercial-NoDerivatives 4.0 International License, which permits any non-commercial use, sharing, distribution and reproduction in any medium or format, as long as you give appropriate credit to the original author(s) and the source, provide a link to the Creative Commons licence, and indicate if you modified the licensed material. You do not have permission under this licence to share adapted material derived from this article or parts of it. The images or other third party material in this article are included in the article's Creative Commons licence, unless indicated otherwise in a credit line to the material. If material is not included in the article's Creative Commons licence and your intended use is not permitted by statutory regulation or exceeds the permitted use, you will need to obtain permission directly from the copyright holder. To view a copy of this licence, visit <http://creativecommons.org/licenses/by-nc-nd/4.0/>.

© The Author(s) 2025